NASA TECHNICAL MEMORANDUM

NASA TM X-1459

NASA TM X-1459

ATLAS-CENTAUR-SURVEYOR LONGITUDINAL DYNAMICS TESTS

by Theodore F. Gerus, John A. Housely, and George Kusic

Lewis Research Center

Cleveland, Ohio

NATIONAL AERONAUTICS AND SPACE ADMINISTRATION • WASHINGTON, D. C. • OCTOBER 1967

NASA TM X-1459

ATLAS-CENTAUR-SURVEYOR LONGITUDINAL DYNAMICS TESTS

By Theodore F. Gerus, John A. Housely, and George Kusic

Lewis Research Center
Cleveland, Ohio

NATIONAL AERONAUTICS AND SPACE ADMINISTRATION

For sale by the Clearinghouse for Federal Scientific and Technical Information
Springfield, Virginia 22151 – CFSTI price $3.00

ATLAS-CENTAUR-SURVEYOR LONGITUDINAL DYNAMICS TESTS

by Theodore F. Gerus, John A. Housely, and George Kusic

Lewis Research Center

SUMMARY

Full-scale dynamics tests were conducted at the NASA Lewis Research Center to investigate engine-structure coupled longitudinal oscillations **(POGO)** of the Atlas-Centaur launch vehicle. Dynamic characteristics determined are natural frequencies, damping ratios, mode shapes, and propellant pressure-force responses.

Experimental values of first mode natural frequencies were in good agreement with analytical values generated by General Dynamics Convair and Rocketdyne Division of North American Aviation, Incorporated. Second mode values were in close agreement for early flight times (near-full tanking condition) but theoretical values were much higher for near-empty tanking conditions. Mode shapes showed reasonably good agreement with the analytical model for this kind of experiment. The greatest discrepancy was found in the modal amplitudes of the propellant masses and propellant pressure-force responses. Structural damping values obtained showed that theoretical minimum requirements for stability of the engine-pump-structure loop are met in all cases, although marginal just before booster engine cutoff. Flight data have confirmed this marginal stability.

INTRODUCTION

Titan 11, Thor, and Jupiter vehicles have exhibited longitudinal oscillations **(POGO)** because of either dynamic characteristics of the engines and propellant feed systems alone or the coupling of engine and structural dynamics. The mechanism for the latter type of disturbance is basically a feedback system involving engine thrust perturbations which excite longitudinal structural modes and cause changes in propellant feed pressure which in turn cause continued thrust perturbations. The following sketch illustrates this loop phenomenon:

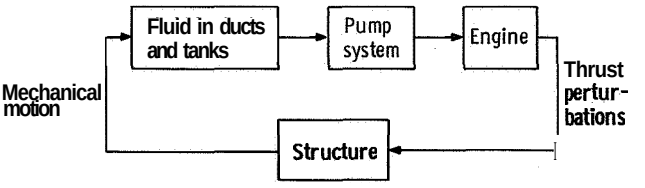

The loop dynamics must meet minimum stability requirements (attenuation and phase shift) in order to avoid sustained oscillations. These oscillations, if of a large magnitude or long duration, could result in engine shutdown and/or destruction of the vehicle.

Although previous Atlas flights have not encountered such phenomena, the addition of the Centaur upper stage changes the structural characteristics considerably. At the request of the NASA Lewis Research Center, analytical studies were conducted by General Dynamics/Convair (ref. 1) and by the Rocketdyne Division of North American Aviation, Incorporated (ref. 2) to investigate the possibility of these oscillations occurring in the Atlas-Centaur vehicle. These studies, based upon theoretical dynamic characteristics of the Atlas-Centaur, indicated that a relatively high degree of structural damping was needed to maintain stability. In an attempt to experimentally verify these analyses, a series of longitudinal dynamics tests on a full-scale Atlas-Centaur vehicle were conducted in a dynamic test facility at the Plum Brook Station of Lewis from November, 1963 to July, 1964. Natural frequencies, mode shapes, damping, and propellant pressure responses were studied. Particular emphasis was placed on determining the characteristics of the liquid oxygen (lox) supply system rather than fuel system, since early analytical studies showed that the lox supply system was the major contributor to POGO instability.

TEST SETUP

The Plum Brook E-site (fig. 1) which had been originally built to test an Atlas vehicle was heightened to accommodate the Atlas-Centaur combination. Test hardware for the first nine tests consisted of the 116-D Atlas, a flight-type interstage adapter, and a rigid water-filled tank (dummy Centaur) having the same mass as the Centaur-Surveyor. The use of a dummy mass was used because of the unavailability of a flight-type Centaur tank in the desired time period. Justification for this decision was based upon an early General Dynamics/Convair study of the Atlas-Centaur structural response which indicated that the upper stage would be moving essentially as a rigid body in the first two longitudinal modes at flight times of interest. When a Centaur tank, insulation panels, nose fairing, and Surveyor model were received, tests 10 to 15 were run with these in place of the dummy Centaur.

To facilitate mating with the suspension system, the Atlas was modified by replacing all structure and components aft of the thrust barrel with an equivalent mass I-beam structure X-frame. A suspender consisting of a steel cable, spring box, hydraulic cylinder, and a load cell was fastened to each of the four frame ends (fig. 2). Each spring box (fig. 3), contained 4 to 16 springs, with a constant of about 400 pounds per inch (7.0×10^4 N/m) per spring. The number of springs for each test was proportioned to the vehicle weight of the particular configuration, in order to give a static deflection of 1 foot (0.3 m), thus keeping the natural frequency of the suspension system well below the range of vehicle resonances. Lateral stability of the system was provided at the bottom by the $1/2^{\circ}$ (8.7×10^{-3} rad) inclination of the cables and at the top by horizontal springs (fig. 2).

In order to avoid operational problems involved with the handling of cryogenic propellants, an equal volume of deionized water was tanked instead of lox and RP fuel, and polystyrene balls having an equivalent bulk density replaced the liquid hydrogen. For testing, the propellant tanks were maintained at flight pressures of 29.5 and 59.0 pounds per square inch gage (2.03×10^5 and 4.06×10^5 N/m^2 gage) in the Atlas lox and fuel tanks, respectively, and 15 and 5 pounds per square inch gage (1.03×10^5 and 3.44×10^4 N/m^2 gage) in the Centaur lox and liquid hydrogen tanks. Inasmuch as a hazardous condition with respect to tank rupture exists at these pressures, it was necessary to control all operations remotely, once the tanking procedures were begun. These remote operations were conducted from a control room (H-building) which was approximately 1/4 mile (400 m) away. Television cameras were used to monitor the vehicle.

INSTRUMENTATION

Instrumentation for tests 1 to 9 (dummy Centaur) consisted of strain-gage-type accelerometers and pressure transducers. Locations on X and Y axes are shown in figure 4. For tests 10 to 15 (actual Centaur) the accelerometers were relocated to cover the Centaur stage and foil-type strain gages were mounted on the Atlas tank skin. Locations are shown in figure 5. Pressures were measured in the lox system by close-coupled strain-gage-type transducers located in the lox system as shown in figure 6. Load cells were used for both vehicle weighing and a measurement of driving force level. All modal data were digitally recorded and reduced with a digital computer program. Sixteen channels of data which were randomly selected were recorded on oscillograph paper. All damping was determined through the use of analog oscillograph paper. End-to-end system accuracy of the instruments is considered to be about 2 percent of full scale. Full-scale ranges of the instruments were as follows:

Accelerometers, g (m/sec^2)	±1.0 (±9.8)
Load cell (force), lb (N)	±1000 (4.45)
Pressure, psia (N/m^2 abs)	0 to 100 (0 to 6.89×10^3)

TEST PROCEDURE

For testing, the Atlas tanks were filled to a level representing 0, 30, 60, 90, 120, 132, 144, or 151 (BECO) seconds of flight time and pressurized to flight pressures. Table I describes the test configurations. Excitation was then applied to the suspended vehicle by an electrodynamic shaker via load cell and X-frame at frequencies varying from 6 to 40 hertz. Input force levels ranged from 500 to 5000 pounds (2.22×10^2 to 2.22×10^3 N) with resulting accelerations of 0.6 g (5.9 m/sec^2) zero-to-peak maximum on the vehicle.

When resonant conditions were determined, transducer output was recorded on analog recorders and on digital tape. Data were taken at discrete points near each resonance peak to define the response curve. At the resonance peak the shaker was electrically decoupled allowing natural decay of the oscillations with transducer output being recorded on the analog recorder. This procedure was followed to identify the first two modes of each tanking condition.

RESULTS AND DISCUSSION

The values of natural frequency obtained in tests made with the dummy Centaur were significantly different from those found in tests with the actual flight-type stage. Although data from both series of tests are presented for comparitive purposes, the discussion is limited to the comparison of experimental results with theoretical analysis using the Centaur tank and SD-4 dummy Surveyor.

Analytical values of natural frequencies and mode shapes are taken from the latest studies performed by General Dynamics/Convair (ref. 1). The theoretical maximum values of pressure-force response reported herein are based on the block diagram of appendix A and make use of analytical mode shapes and modal masses and experimentally determined values of damping.

Natural Frequencies

Figure 7 compares theoretical and experimental natural frequencies of the Atlas-Centaur-Surveyor for the first two longitudinal modes. The first modal frequencies appear to agree very well but divergence between the second mode predicted and measured frequencies indicate some analysis limitations. The second mode frequencies agree very well at the time of predicted second mode POGO (30-sec flight time). Also shown in figure 7 are experimental Atlas-dummy Centaur data, illustrating the inaccuracies in natural frequencies resulting from assuming Centaur a rigid body.

The first mode resonance at 90 seconds and the second mode resonance at 151 seconds were not found. In the first case it is believed that coincidence of a node with the point of force input prohibited modal excitation. In the latter case an area of weak vehicle response was noted at about $16\frac{1}{2}$ hertz which was probably the second mode, but the transducer signals were of such low strength and poor quality that the actual peak response could not be accurately determined.

Mode Shapes

Relative movement of vehicle segments was determined directly from accelerometer outputs except for lox and fuel mass motions which were determined from strain gage data by the method of appendix B. A comparison of modal amplitudes for the first two longitudinal modes is shown in tables II and III. It should be noted here that the amplitudes represented are the vector sum of real and imaginary components with the sign determined by the direction of the real component relative to the maximum amplitude, arbitrarily set at +10. Although most data had very small imaginary amplitudes (relative to maximum amplitude), no attempt will be given in this report to separate the real and imaginary terms.

The differences between theoretical and experimental modal deflections are smallest for the first mode early flight times and largest for second mode late flight times. This is common with analytical modeling of structural modes. The following is a list of possible sources of differences between the analytical and experimental mode shapes (no relative significance is given here for these suggested differences):

(1) Representation of fuel and lox as single masses with skins deflected as a truncated cone. Strain gage data indicate this assumption fair for lower modes but questionable for higher modes. Figures 8 and 9 show the hoop strain resulting from longitudinal oscillations,

(2) Measurement and computation accuracy. Since fuel and lox modal deflection are computed by using hoop strain gages with assumptions as given in appendix B, some limitation in accuracy is probable. Other normal instrument accuracies as given in the instrument section may also contribute.

(3) Finite mass and spring assumptions. Although it is customary to break a continuous system into finite springs and masses, the degree of accuracy is always limited by the choice of the separation. Figures **10** and **11** show outputs of accelerometers mounted on the tank skin for each mode which show continuous motions of masses. It should be noted that these are plotted in a lateral plane to show longitudinal acceleration.

(4) Normal mode assumptions in analytical model. In the analytical model there are no imaginary vectors when the mass modal deflections are computed. It is generally impossible to excite a true normal mode experimentally, especially with a single force exciter.

(5) Suspension system limitations. Although a great deal of care was taken in the design of the suspension system, it is not a true free-free system.

(6) Nonlinearities and Poisson's ratio effect. All equations in the analysis are assumed linear. Damping data in the next section show these limitations. Poisson's ratio is not included in the analysis.

Damping

Standard technique of analysis of decay curves (of which fig. **12** illustrates several typical) shows that the decay is not exponential and that both viscous and coulomb damping are present. Although the concept of critical damping is based on a viscously damped second order system, an equivalent value for this system may be determined by basing the logarithmic decay computation on the number of cycles required to decay from maximum to near zero amplitude. Damping ratios obtained by this method meet theoretical minimum requirements for stability in all cases. It is interesting to note that first mode small amplitude POGO oscillations **(0.125-g (1.23** m/sec^2) zero-peak (ref. **3))** occurred at the time when stability margins are smallest, but second mode POGO occurred when analysis indicated a high stability margin. This indicates that the second mode accuracy is less than that of the first mode. Data shown in figure **13** indicate damping measured in Atlas-Centaur tests ranging from **1.1** percent of critical to **4.8** percent of critical at liftoff and Booster Engine Cutoff, respectively. Missing data points occur where either no mode was found or where the decay curve was of poor quality. Figure **14** indicates damping measured in Atlas-dummy Centaur tests for comparitive purposes.

Evidence that the damping characteristics may be undergoing a softening characteristic with force (less damping with greater amplitude, ref. **4)** is indicated by the shifts in

peaks in figure 15. Here it will be noticed that an increase in force causes a greater than proportional increase in amplitude and that the frequency of peak response is lowered. The range of accelerometer response for this data is from 0 to 0.5 g (4.9 m/sec^2) in comparison with the 0.125 g (1.23 m/sec^2) seen in flight. It was suggested that the source of this effect might be the polystyrene balls used in the Centaur hydrogen tank and/or Centaur insulation panels, but an additional test run with the tank empty and no insulation panels showed insignificant difference in damping values.

Lox Duct Pressure Responses

Transducers mounted in the main lox line and at the capped ends of pump feed lines as shown in figure 6 were used to determine pressure/force responses. Although data were obtained for all cases, only one portion of the flight is shown here, arbitrarily chosen as 60-second flight time. The analytical data shown were based upon theoretical mode shapes and experimentally measured damping (appendix B). The pressure responses were computed for a nonflowing liquid, specifically the E-stand configuration. Figures 16 to 19 show analytical values much higher than those measured in the tests. Furthermore, the sustainer and booster lox pump inlet pressures measured show a rise in pump inlet pressures below structural responses. These data are difficult to interpret since the lines could not be mechanically terminated in the same way as they are in flight. Part of the difference in response could be attributed strictly to unrealistic motion of the pipes themselves. Experimental and theoretical values for the 60-second flight time (figs. 16 to 19) show the analytical values to be orders of magnitude higher in the first mode and by as much as 20 to 1 in the second mode. These discrepancies were typical for all tests.

With an exciting frequency near 6 hertz, high pressure was noted in the lox feed lines. This is attributed to a pipe resonance since the frequency did not coincide with a vehicle natural frequency and did not occur in the lox tank bottom.

Theoretical data presented for comparison are based on the Plum Brook configuration (i.e., no engines, no flow, and water in tanks). A block diagram describing the various dynamic terms for the configuration is presented in appendix B.

CONCLUSIONS

The test data presented show a close correlation with predicted frequencies and a reasonable correlation with mode shapes for this kind of experiment. Although the analytical models used for comparison were the most recent models generated by General

Dynamics/Convair, upgrading is continuing in an effort to make the structural analytical model as accurate as possible. With the present analytical model of the structure, measured damping, and calculated line and engine responses, it is possible to generate a stability limit that closely agrees with flight data in the first mode. However, since no reasonable measurements have been made coupling fluid lines and pumps, it is felt that any further test activity should be in this direction.

Lewis Research Center,
National Aeronautics and Space Administration,
Cleveland, Ohio, June 15, 1967,
491-05-00-01-22.

APPENDIX A

LOX TANK PRESSURE SYSTEM E-STAND CONFIGURATION

The following block diagram is the analytical model of the part of the loop used for the E-stand test configuration. This is part of the loop used in the complete system analytical model and modified for use here. P* is the pressure derived from the force considering the sum of the structural response of the aft end of the vehicle and the lox mass. P_J, P_1, P_2, and P_s are pressures computed utilizing P* and the response of the ducts.

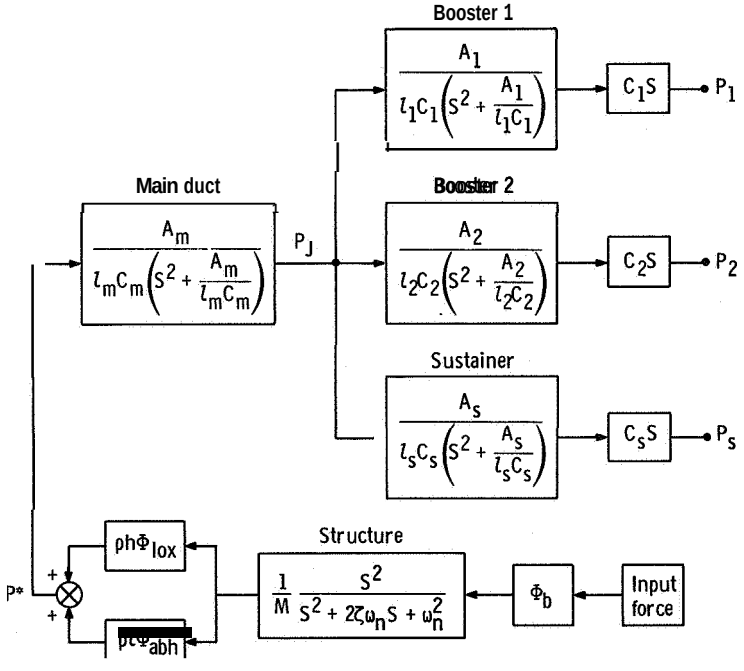

APPENDIX B

METHOD FOR COMPUTING FLUID MASS MOTION FROM STRAIN GAGE DATA

This analysis assumes that the tank bottom is rigid and that strain between gages has a linear distribution. As shown in the sketch at the left, longitudinal oscillations will cause a change in tank volume, due to pressure fluctuation on the tank wall as given by $\Delta P = \ddot{\chi} h \rho$ where $\ddot{\chi}$ is the induced acceleration, h is the height of liquid, and p is the density of liquid. (Symbols are defined in appendix C.) Strain gages located on the tank skin may be used to compute the resulting motion of the liquid center of gravity. The change in area of any section is given with good accuracy by

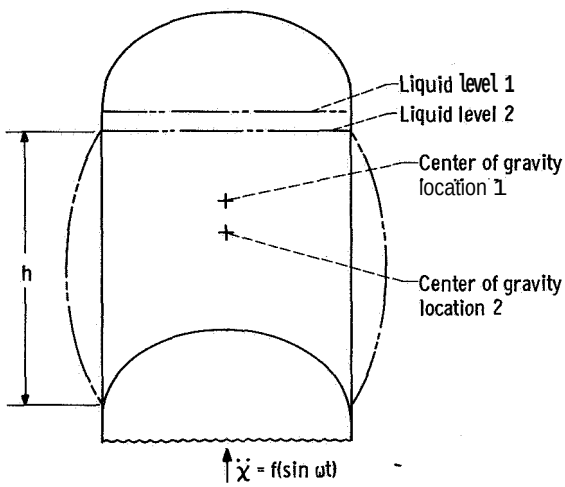

$$AA = 2\pi R(\Delta R)$$

where AR is a function of hoop strain (see sketch at left) and is given by

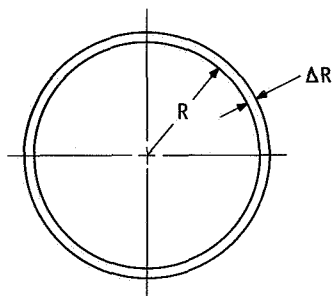

$$AR = \frac{A\ \text{circumference}}{2s} = \frac{\epsilon(2\pi R)}{2a}$$

Where ϵ is unit strain, then

$$AA = R\epsilon(2\pi R)$$

With a pressure distribution as shown in the sketch at the left where $\epsilon_1, \epsilon_2, \cdots, \epsilon_8$ are measured hoop strains, the volume change is given by

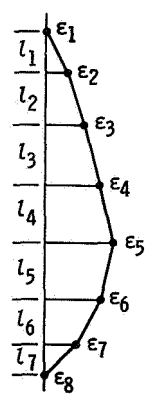

$$\Delta V = 2\pi R^2 \sum_{n=1}^{n=7} \left(\epsilon_n + \frac{\epsilon_{n+1} - \epsilon_n}{2} \right) l_n \qquad (A1)$$

The change in height of liquid will then be given by

$$\Delta h = \frac{\Delta V}{\pi R^2}$$

and the change in center of gravity location is β Ah where β is a coefficient which considers tank geometry such as dome or cone bottoms. The sensitivity of β to liquid level for the Atlas tanks is shown in the sketch at the left. When sinusoidal motion is assumed, the acceleration with respect to the tank bottom is

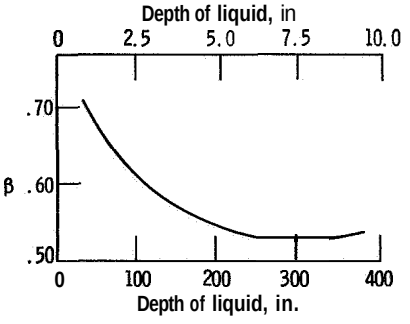

$$|\ddot{x}| = \beta \frac{\Delta V}{\pi R^2} \omega^2 \qquad \text{(A2)}$$

where ω is the circular frequency. Combining equations (Al) and (A2) results in

$$|\ddot{x}| = 2\beta\omega^2 \sum_{n=1}^{n=7} \left(\epsilon_n + \frac{\epsilon_{n+1} - \epsilon_n}{2}\right) \zeta n \qquad \text{(A3)}$$

The total acceleration of the center of gravity is then the sum of equation (A3) and the acceleration of the tank bottom.

APPENDIX C

SYMBOLS

A	cross sectional area of **lox** duct, in.^{2} (m^2)
C	capacitance of duct, in.-sec^2 (m-sec^2)
h	depth of liquid in Atlas lox tank, in. (m)
l	length of duct, in. (m)
M	generalized mass of structural mode being considered, (lb)(sec^2)/in. (kg)
P	pressure at pump inlet, psi (N/m^2)
P*	pressure at top of main duct, psi (N/m^2)
P_J	pressure at bottom of main duct, psi (N/m^2)
R	radius of tank, in. (m)
S	Laplacian operator, sec^{-1}
V	volume of tank, in.^{3} (m^3)
E	unit strain, in. (m)
ζ	damping ratio, dimensionless
P	density of water, lb/in.^{3} (N/m^3)
Φ_{abh}	modal amplitude of aft bulkhead, dimensionless
Φ_b	modal amplitude of gimbal plane, dimensionless
Φ_{lox}	modal amplitude of lox mass, dimensionless
$\ddot{x}$	induced acceleration, g (m/sec^2)
ω	circular frequency, rad/sec
ω_n	undamped natural frequency, rad/sec

Subscripts:

m	main lox duct
s	sustainer engine lox duct
1	engine 1 booster lox duct
2	engine 2 booster **lox** duct

REFERENCES

1. Rose, Robert G.; Simson, Anton K.; and Staley, James A.: A Study of System-Coupled Longitudinal Instabilities in Liquid Rockets. Part 1: Analytic Model. Rep. No. GD/C-DDE65-049, pt. 1 (AFRPL-TR-65-163, pt. 1, DDC No. AD-471523), General Dynamics/Convair, Sept. 1965.

2. Wolf, K. E.; Austin, E. A. and Nelson, R. L.: Study of Longitudinal Oscillations During Flights of Atlas Space Launch Vehicles. Rep. No. AER 64-2, Rocketdyne Div., North American Aviation, Inc., Mar. 30, 1964.

3. Staff of Lewis Research Center: Post Flight Evaluation of Atlas-Centaur AC-4 (Launched December 11, 1964). NASA TM X-1108, 1965.

4. Harris, Cyril M.; and Crede, Charles E., eds.: Shock and Vibration Handbook Vol. 1. McGraw-Hill Book Co., 1961.

TABLE I. - TEST CONFIGURATIONS

Pest	'light, :ime, sec	Volume of water n Atlas fuel tank, V_F		Volume of water n Atlas lox tank, V_L		Configuration	Total test weight	
		ft3	m^3	ft3	m^3		lb	kg
1	-----	0	0	0	0		29 400	13 336
2	151.7	151	4.28	221	6.26		67 990	30 840
3	144	197	5. 58	298	8.43		75 670	34 323
4	132	307	6.69	461	13.6		93 950	42 615
5	120	416	11.6	663	18.8		112 110	50 852
6	90	723	20.5	1113	31.5		159 350	72 280
7	60	958	27.1	1562	44.2		202 030	91 639
8	30	1227	34.7	2015	57.1		247 270	112 159
9	0	1494	42.3	2473	70.0		292 320	132 593
10	60	956	27. 1	1562	44.2		202 030	91 639
11	151.7	151	4.28	221	6.26		67 990	30 840
12	144	197	5.58	298	8.43		75 670	34 323
13	0	1494	42.3	2473	70.0		292 320	132 593
14	90	723	20.5	1113	31. 5		159 350	72 280
[b]15	151.7	151	4.28	221	6.26		66 610	30 214

[a] Centaur tanks (configuration 2) contained 4630 lb (2100 kg) of polystyrene balls (LH_2) and 310 cu ft (8.77 cu m) of water (LO_2).

[b] Run without insulation panels.

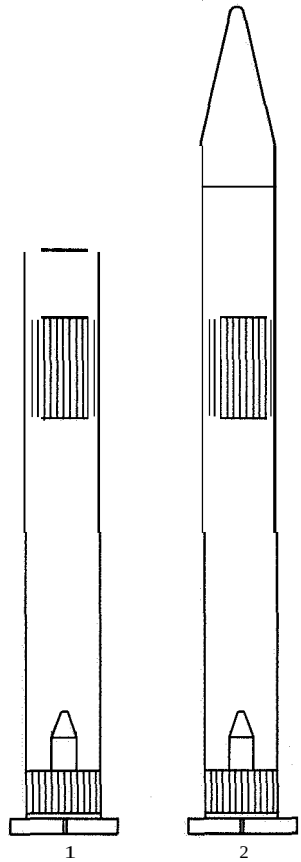

1 2

Configuration

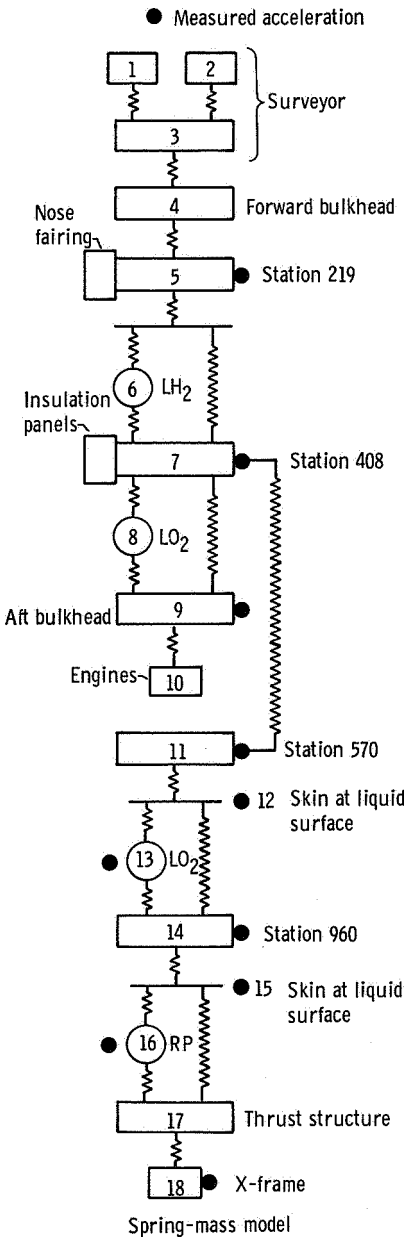

Spring-mass model

TABLE II. - FIRST MODE RELATIVE AMPLITUDE

[No experimental data for 90-second flight time.]

Mass number	Theoretical	Experimental	Theoretical	Experimental	Theoretical	Experimental	Theoretical	Experimental
	Flight time, sec							
	0		60		144		151	
5	0.697	0.39	0.959	0.80	0.906	0.81	-0.752	0.82
7	.679	.40	.912	.86	.797	.75	-.643	-.73
9	.713	.42	1.00	.95	1.00	1.00	-.838	-1.00
11	.615	.31	.750	.66	.436	.31	-.300	-.28
12	-----	----	.608	.62	-.365	-.21	.501	.36
13	-.836	-.14	-.928	-.058	-.926	-.73	1.00	.68
14	.687	.58	.526	.71	-.52	-.60	.615	.59
15	-----	----	.589	.83	-----	----	-----	-----
16	1.00	1.00	.763	.99	-----	----	-----	-----
17	.829	.72	.679	.98	-.636	-.77	.741	.85
18	.840	.73	.694	1.00	-.672	-.79	.790	.88

TABLE III. - SECOND MODE RELATIVE AMPLITUDE

Mass number	Theoretical	Experimental	Theoretical	Experimental	Theoretical	Experimental	Theoretical	Experimental
	0		60		90		144	
5	0.937	0.83	-0.926	-0.83	-0.794	-0.84	-0.95	-0.16
7	.865	.85	-.841	-.82	-.703	-.80	-.061	-.12
9	1.000	1.00	-1.00	-1.00	-.872	-1.00	-.121	-.12
11	.619	.56	.556	.49	-.402	-.44	.034	-.04
12	-----	-----	-.307	-.29	.001	-.06	.235	-.19
13	.038	-.13	-.045	-.02	-.296	-.05	.801	-.10
14	-.042	-.056	-.269	.22	.535	.44	-.410	.25
15	-----	-----	.359	.37	.768	.64	------	-----
16	-.336	-.077	-.616	.56	1.00	.76	------	-----
17	-.167	-.073	-.489	.48	.891	.96	.851	.98
18	-.172	-.085	.510	.49	.953	.96	1.00	1.00

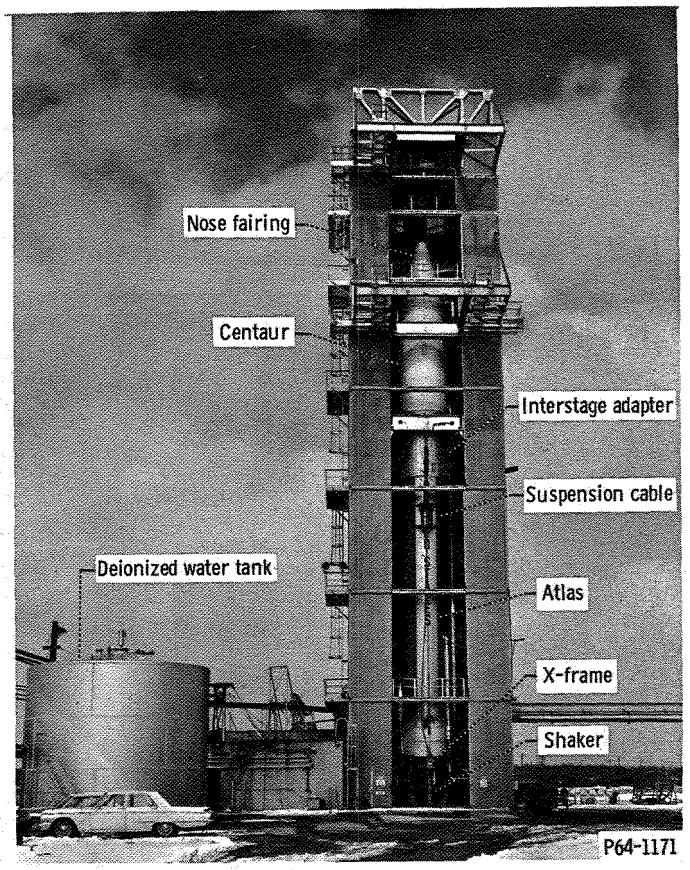

Figure 1. - E-stand test facility with Atlas-Centaur-Surveyor.

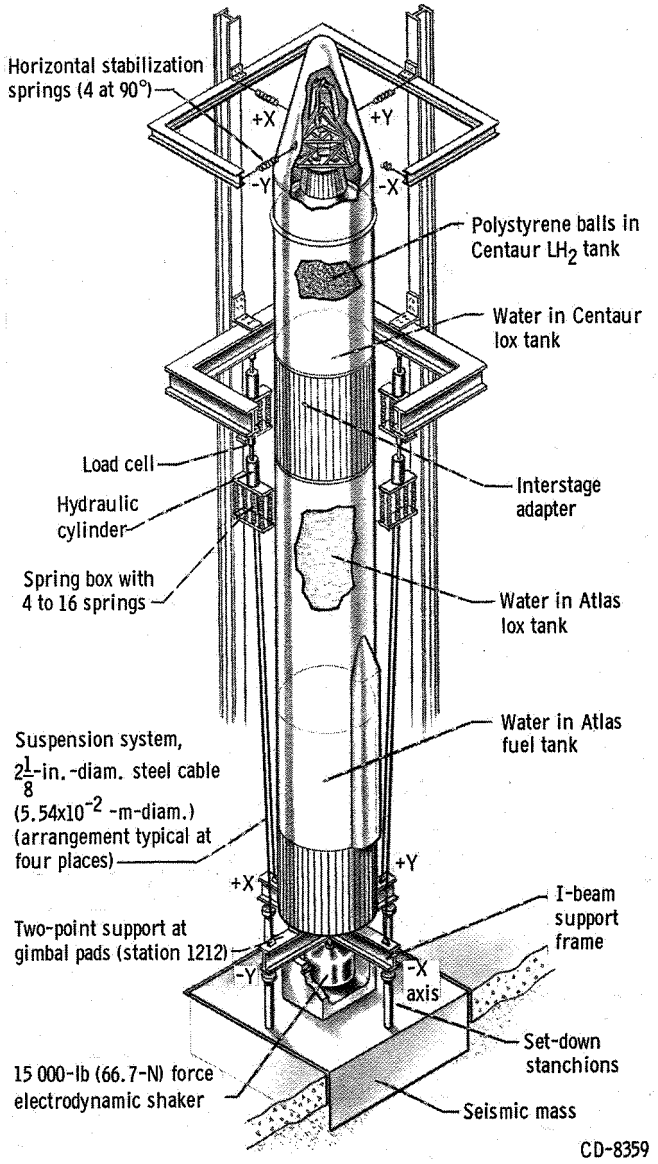

Figure 2. - Vehicle support system.

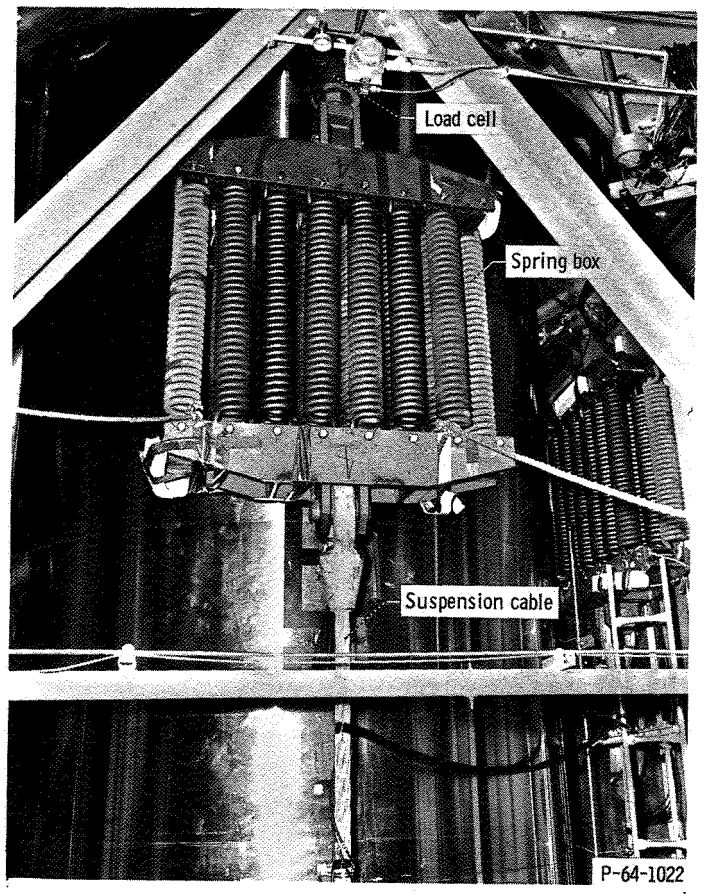

Figure 3. - Closeup of suspension springs.

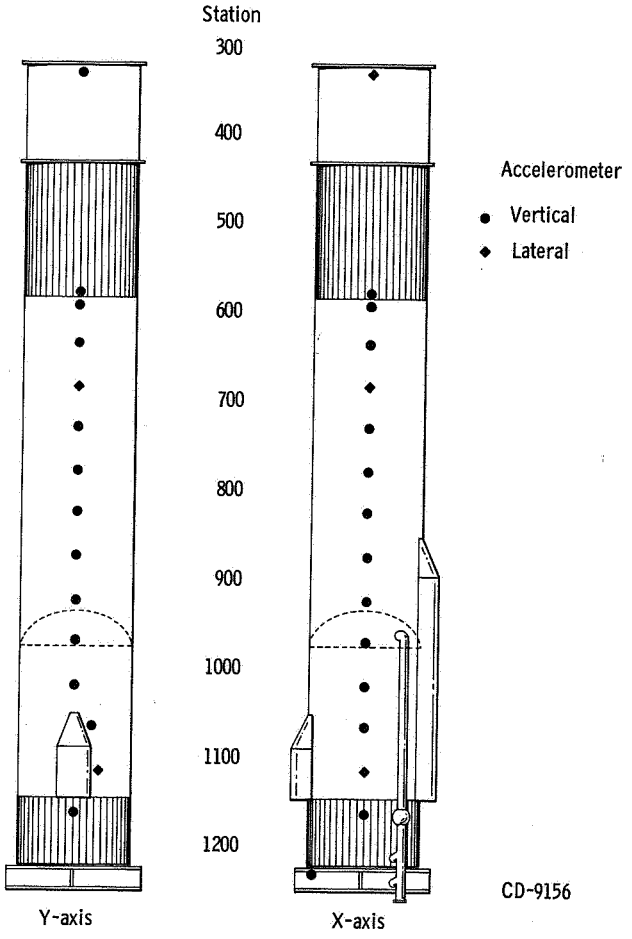

Figure 4. - Instrumentation (tests 1 to 9). Pressure transducers at fuel cone apex, lox line butterfly valve, and lox line upper valve.

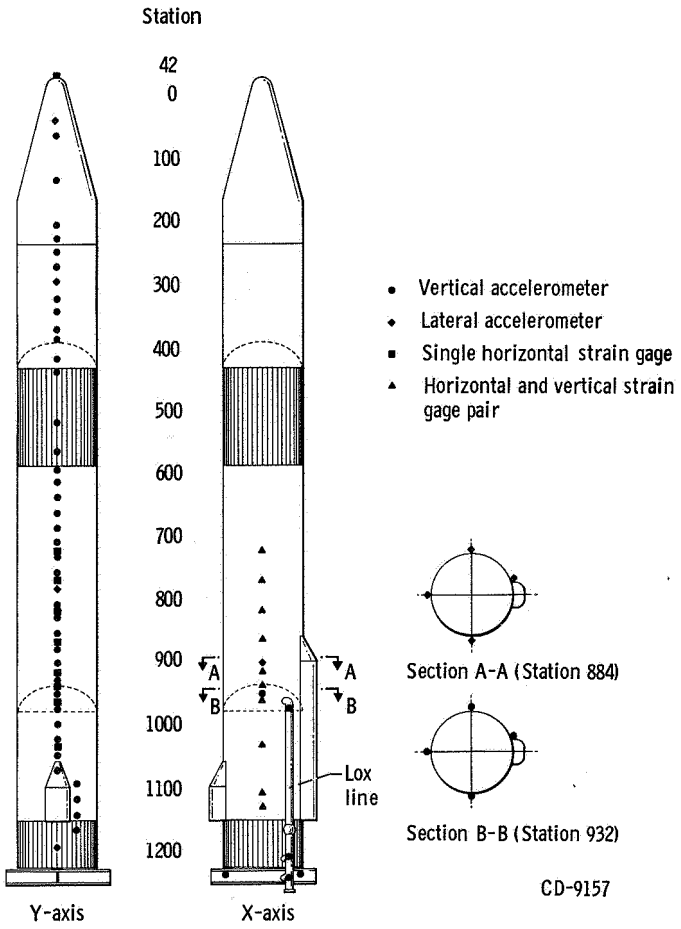

Figure 5. - Instrumentation (tests 10 to 15). Pressure transducers located on lox line at upper valve, butterfly valve, and booster and sustainer engine feed line ends. Pressure transducer at Atlas fuel cone apex.

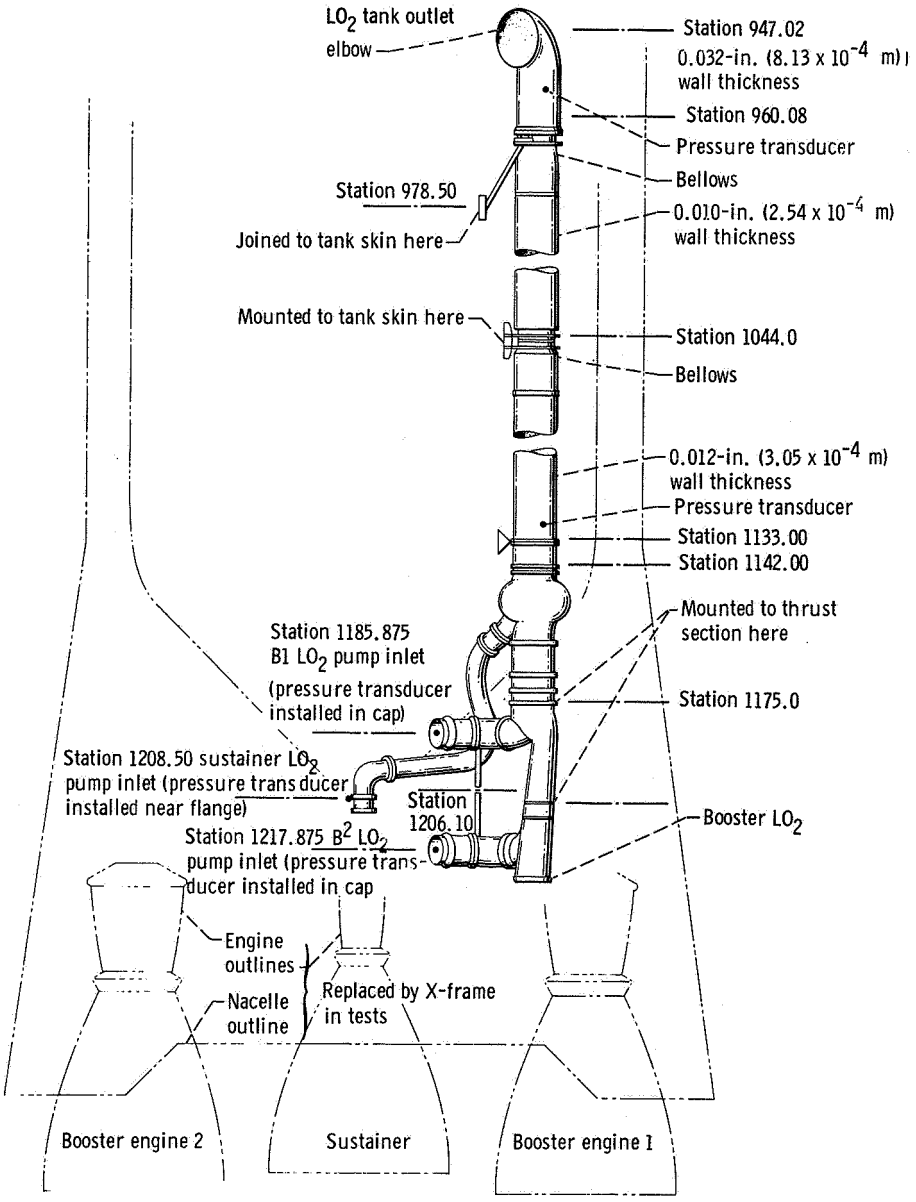

and instrumentation used in tests.

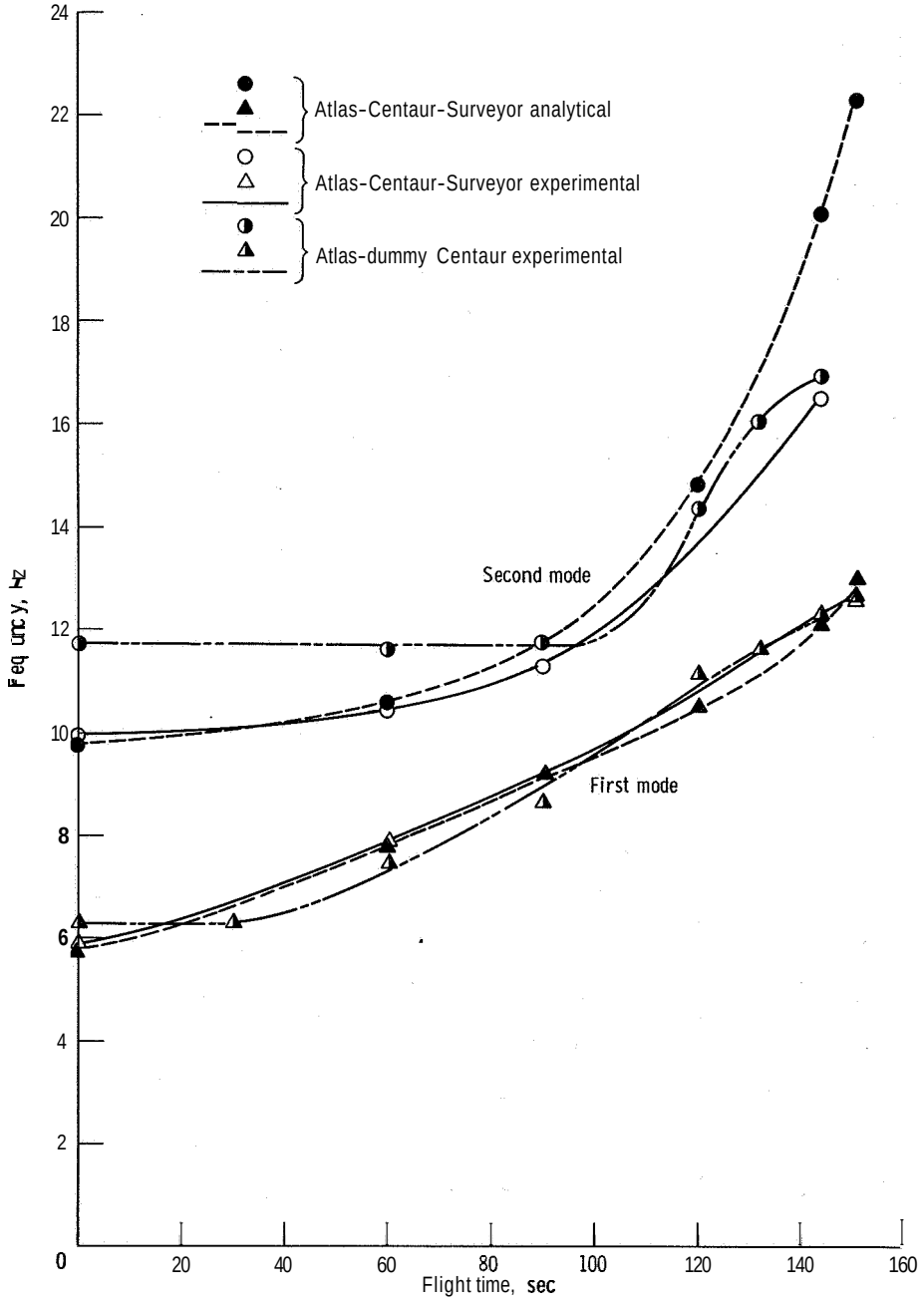

Figure 7. - Natural frequency plotted against flight time for Plum Brook configuration.

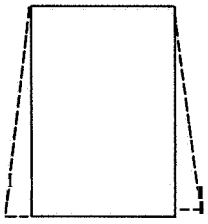

Spring-mass model analysis assumes that displaced tank skin takes form of truncated cone as above

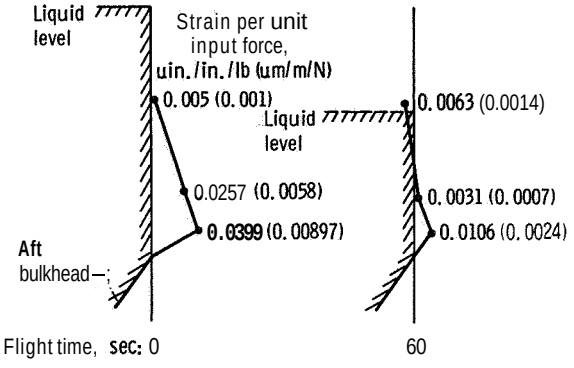

(a) First mode.

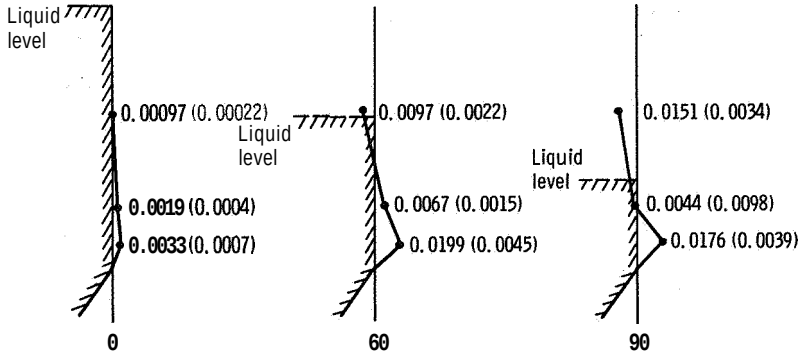

(b) Second mode.

Figure 8. - Atlas fuel tank hoop strain at resonance.

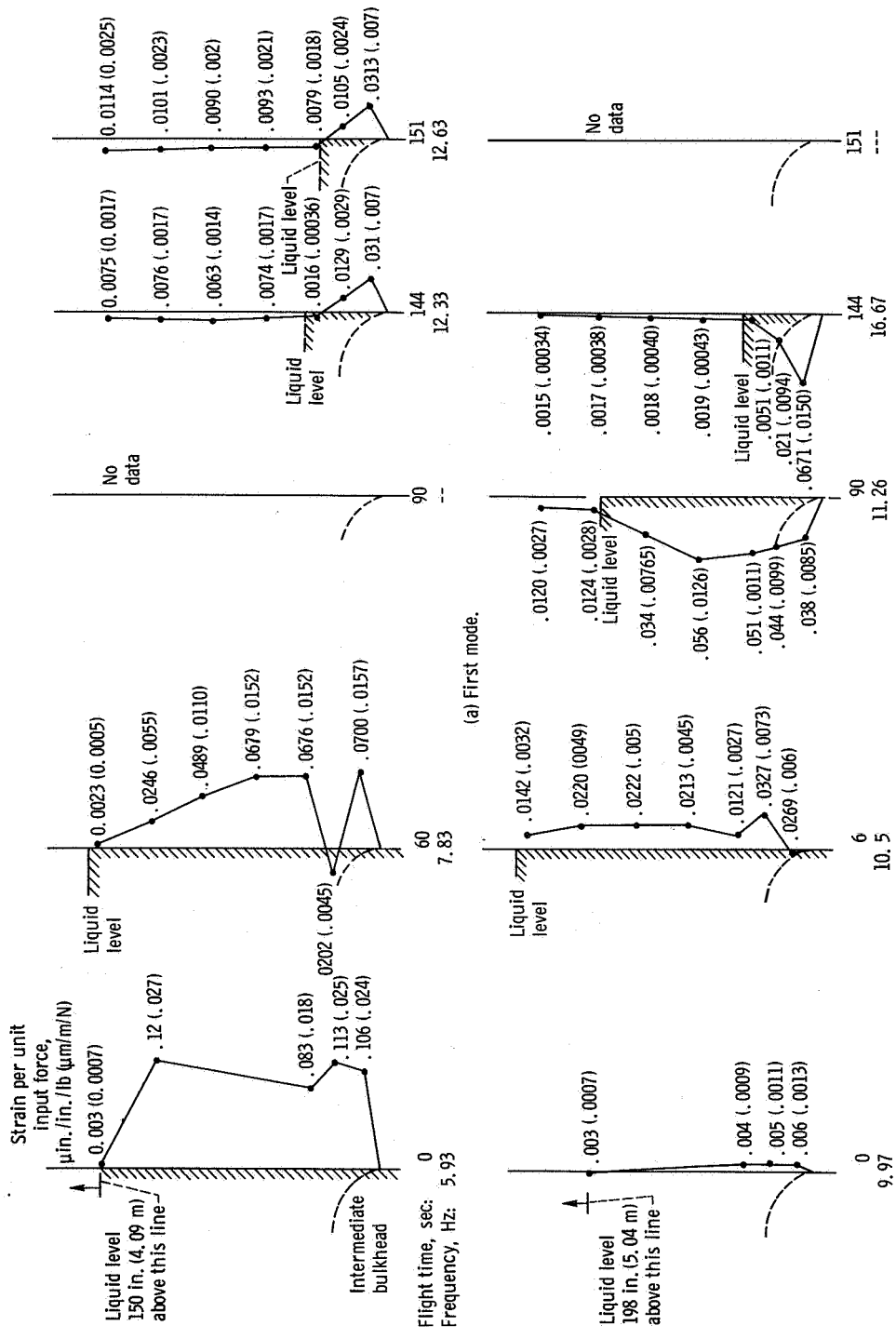

Figure 9. - Atlas lox tank hoop strain at resonance. (Vertical - not to scale).

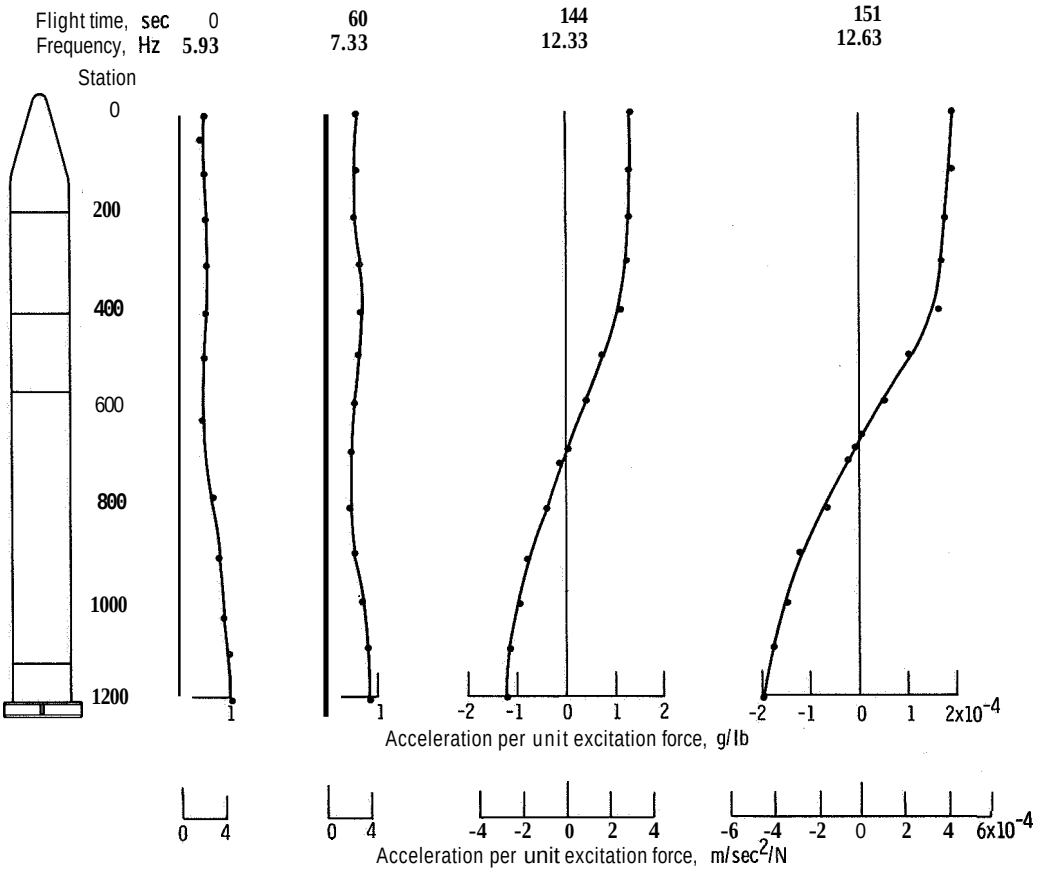

Figure 10. - First mode longitudinal acceleration plotted against station.

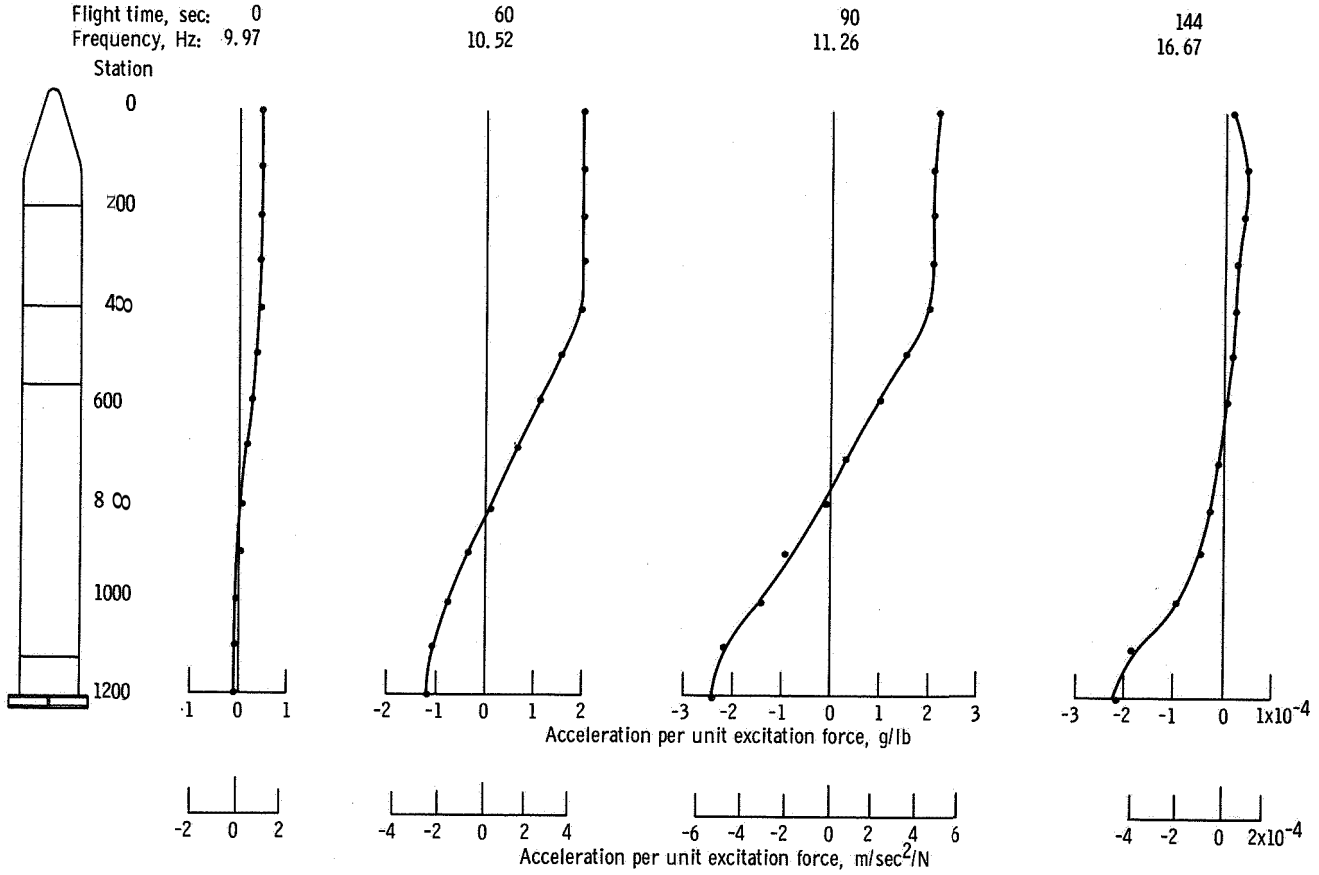

Figure 11. - Second mode longitudinal acceleration plotted against station.

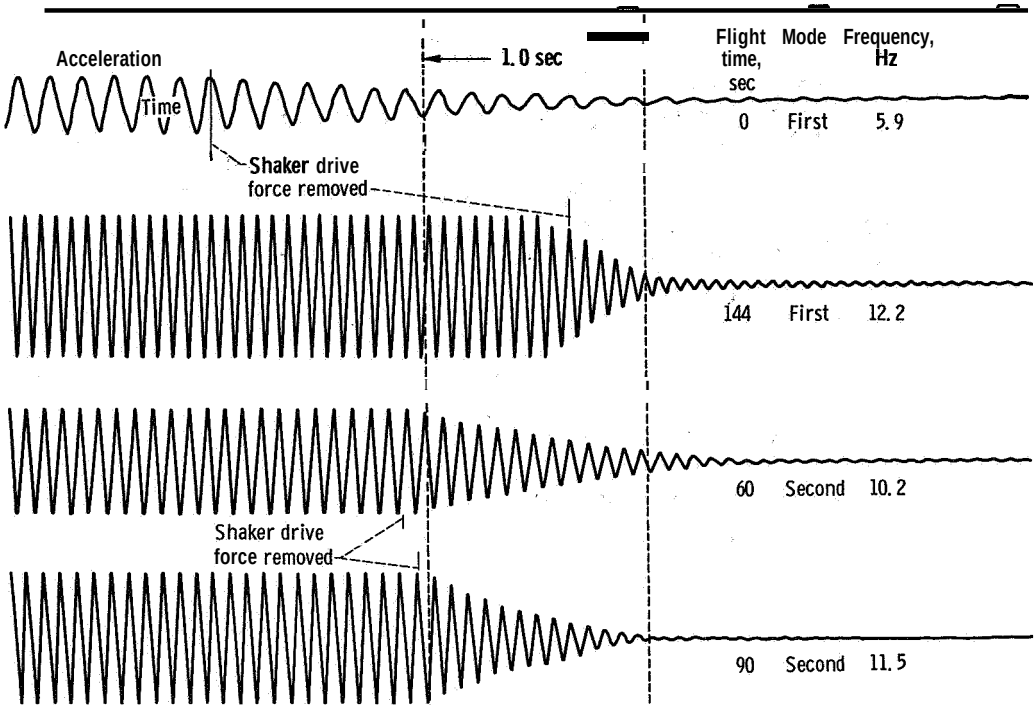

Figure 12. - Atlas-Centaur-Surveyor test stand typical data used to calculate damping by decay methods.

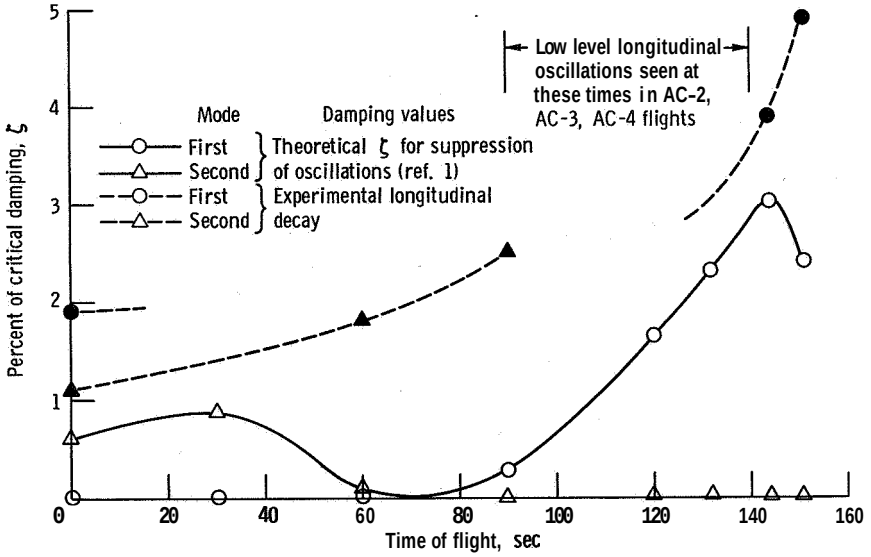

Figure 13. - Damping variations with flight time.

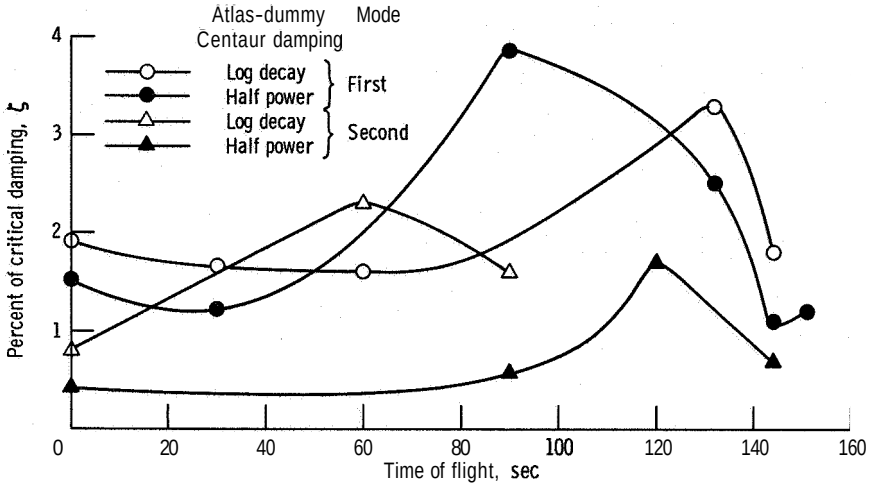

Figure 14. - Atlas-dummy Centaur damping variations with flight time.

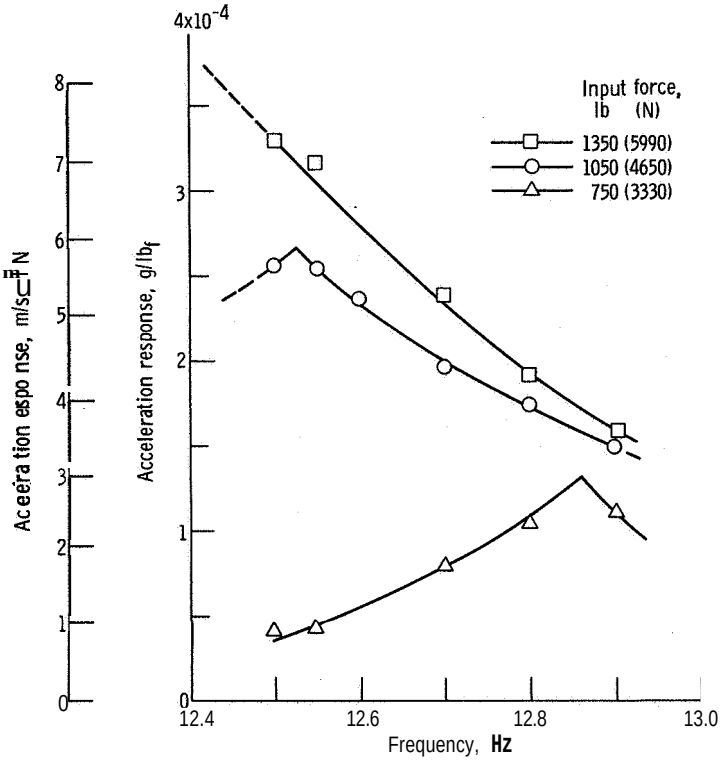

Figure 15. - First mode response. Test 11; booster engine cutoff condition (151 sec).

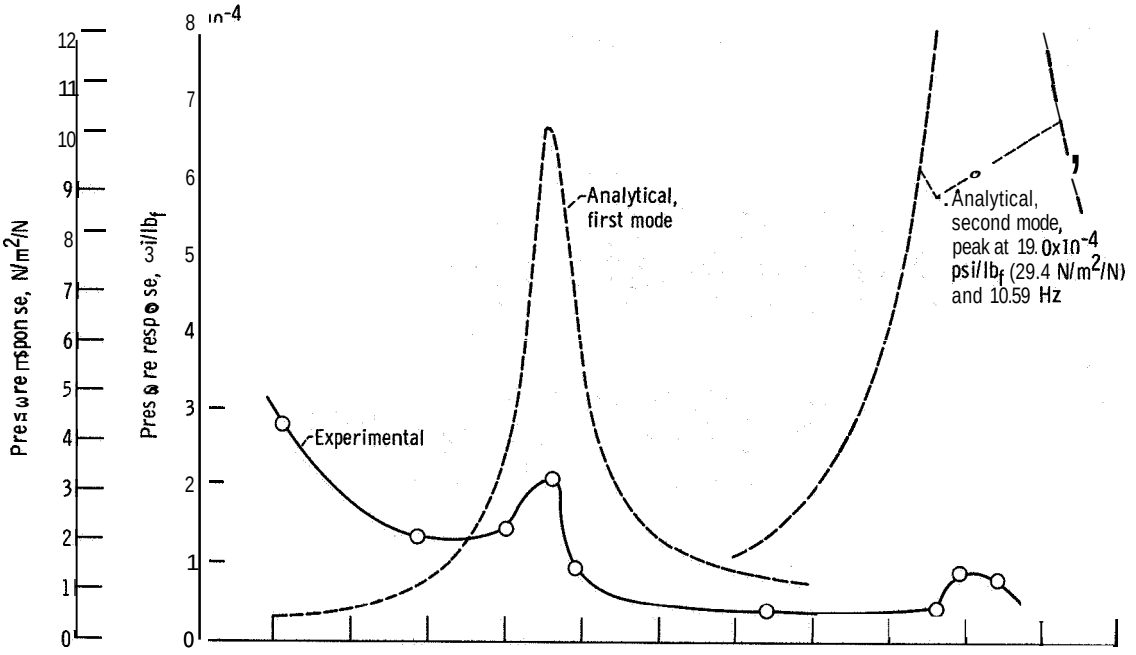
Pressure response, N/m²/N
Pressure response, psi/lbf
Analytical, first mode
Analytical, second mode, peak at 19.0x10⁻⁴ psi/lbf (29.4 N/m²/N) and 10.59 Hz
Experimental

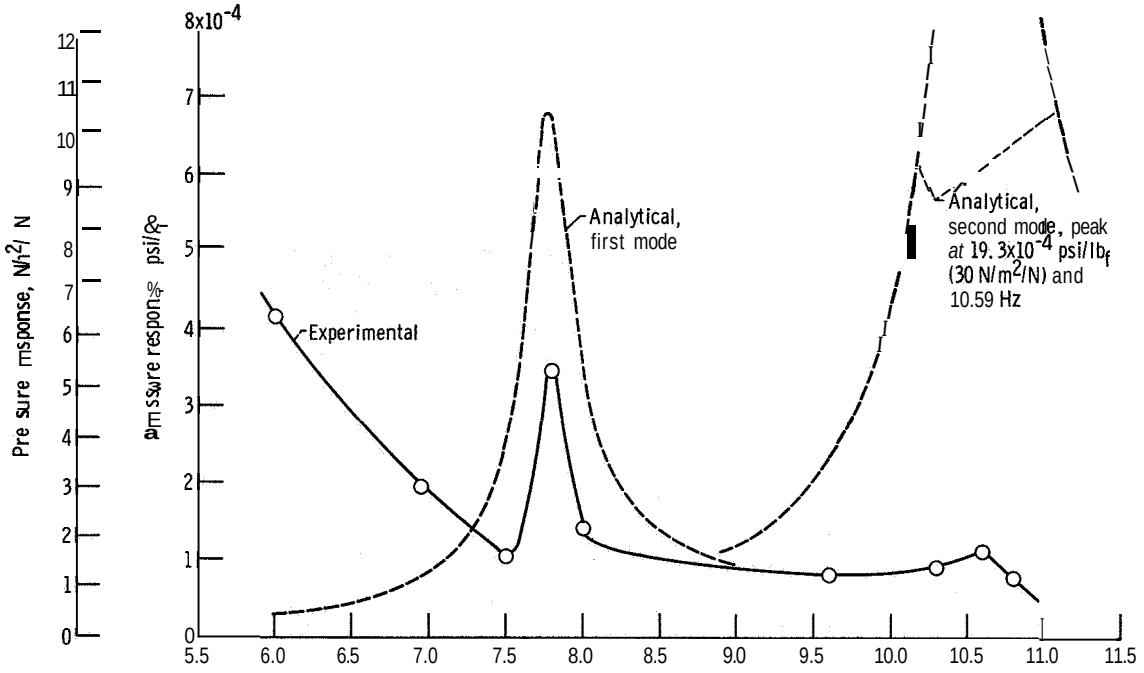
Pressure response, N/m²/N
Pressure response, psi/lbf
8x10⁻⁴
Analytical, first mode
Analytical, second mode, peak at 19.3x10⁻⁴ psi/lbf (30 N/m²/N) and 10.59 Hz
Experimental
5.5
6.0
6.5
7.0
7.5
8.0
8.5
9.0
9.5
10.0
10.5
11.0
11.5

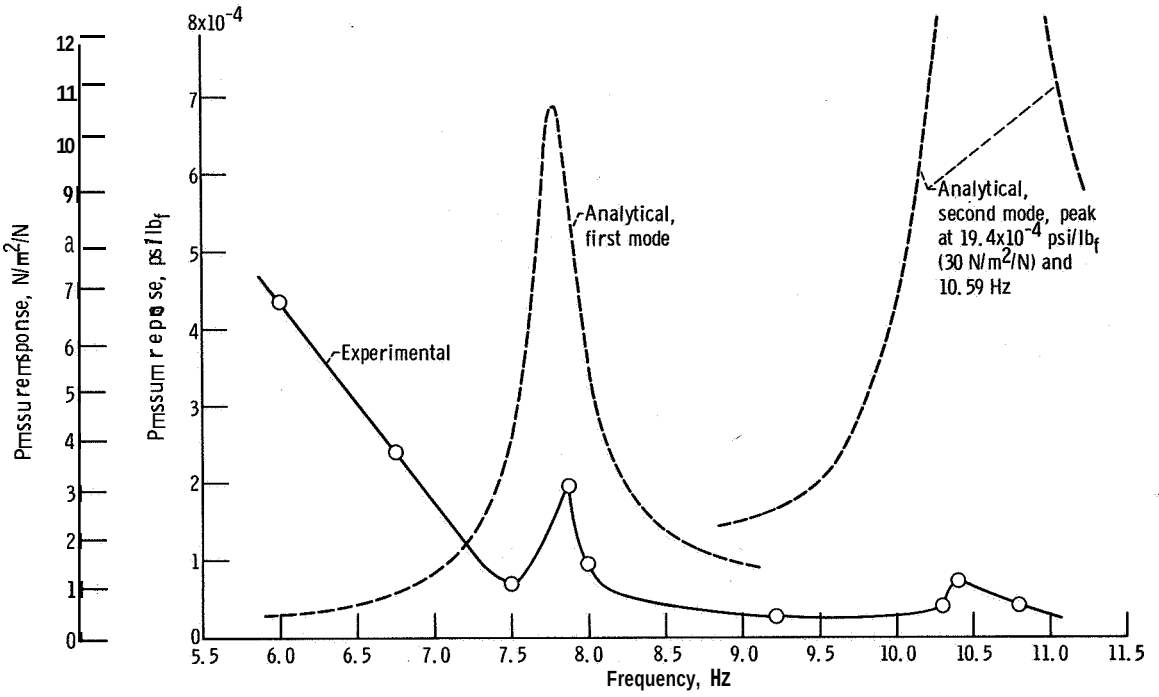

Figure 18. - Sustainer engine lox pump inlet pressure plotted against frequency. Test 10; flight time, 60 seconds.

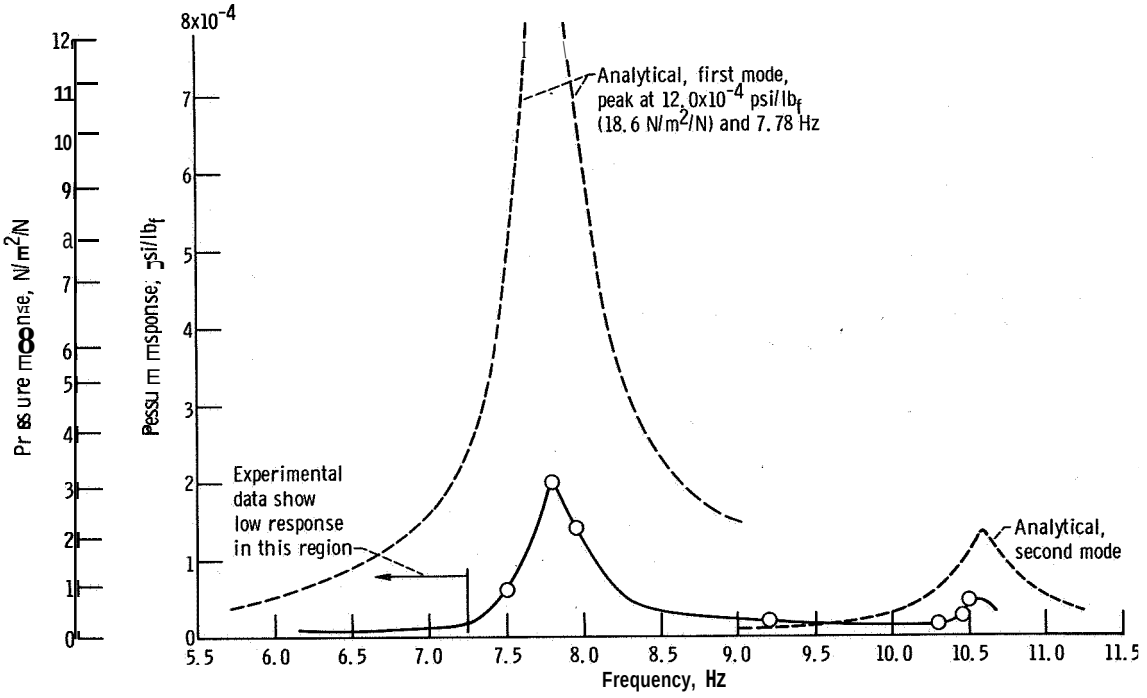

Figure 19. - Lox tank bottom pressure plotted against frequency. Test 10; flight time, 60 seconds.

"The aeronautical and space activities of the United States shall be conducted so as to contribute . . . to the expansion of human knowledge of phenomena in the atmosphere and space. The Administration shall provide for the widest practicable and appropriate dissemination of information concerning its activities and the results thereof."

—National Aeronautics and Space Act of 1958

NASA SCIENTIFIC AND TECHNICAL PUBLICATIONS

TECHNICAL REPORTS: Scientific and technical information considered important, complete, and a lasting contribution to existing knowledge.

TECHNICAL NOTES: Information less broad in scope but nevertheless of importance as a contribution to existing knowledge.

TECHNICAL MEMORANDUMS: Information receiving limited distribution because of preliminary data, security classification, or other reasons.

CONTRACTOR REPORTS: Scientific and technical information generated under a NASA contract or grant and considered an important contribution to existing knowledge.

TECHNICAL TRANSLATIONS: Information published in a foreign language considered to merit NASA distribution in English.

SPECIAL PUBLICATIONS: Information derived from or of value to NASA activities. Publications include conference proceedings, monographs, data compilations, handbooks, sourcebooks, and special bibliographies.

TECHNOLOGY UTILIZATION PUBLICATIONS: Information on technology used by NASA that may be of particular interest in commercial and other non-aerospace applications. Publications include Tech Briefs, Technology Utilization Reports and Notes, and Technology Surveys.

Details on the availability of these publications may be obtained from:

SCIENTIFIC AND TECHNICAL INFORMATION DIVISION

NATIONAL AERONAUTICS AND SPACE ADMINISTRATION

Washington, D.C. 20546